Thermal feedback on wind-stress as a contributing cause of the Gulf Stream[1]

by David Behringer,[2] Lloyd Regier[3] and Henry Stommel[4]

ABSTRACT

A simple model is used to explore a feedback mechanism which may be significant in the formation of the Gulf Stream. The feedback operates through the drag coefficient which is a function of the sea-air temperature difference. The model is divided into interior and western boundary regions which are overlaid by an atmosphere with a constant meridional temperature gradient. The model predicts the interior sea-air temperature difference which determines, in sequence, the enhancement of the basic wind-stress distribution, the interior Sverdrup velocity, and the zonal velocity between the interior and the western boundary regions. All variables are functions of latitude only. Calculations for a two gyre ocean demonstrate the ability of the feedback mechanism to produce a "Gulf Stream" without higher order dynamics.

1. Introduction

The chart of Sverdrup transport (reproduced in Fig. 1) recently published by Leetmaa and Bunker (1978), based on recent recomputations of the wind-stress, shows a well developed Gulf Stream extending out from Cape Hatteras to about longitude 50W—much the same as the Gulf Stream which appears in the dynamic topography (Stommel, Niiler, and Anati, 1978). This is surprising because conventionally we have attributed the narrowness of the Gulf Stream to the operation of higher order dynamical processes, not to fine-structure in the mean wind-stress.

The new fine-structure depicted by Leetmaa and Bunker arises partly from their use of a variable drag coefficient in computing the wind-stress. Using averages of observations between 65W and 70W, they computed a wintertime drag coefficient which is nearly constant at about 1.6×10^{-3} between 21N and 27N but which increases sharply to about 2.2×10^{-3} in the warm core of the Gulf Stream at 37N. They found that using a variable drag coefficient in place of a constant coefficient made little difference in the wind-stress south of the Gulf Stream but caused a 20% to 25% increase in the stress over the Stream. This change occurs abruptly within

1. Contribution No. 4251 from Woods Hole Oceanographic Institution.
2. Atlantic Oceanographic and Meteorological Laboratories, Miami, Florida, 33149, U.S.A.
3. Scripps Institution of Oceanography, La Jolla, California, 92093, U.S.A.
4. Woods Hole Oceanographic Institution, Woods Hole, Massachusetts, 02543, U.S.A.

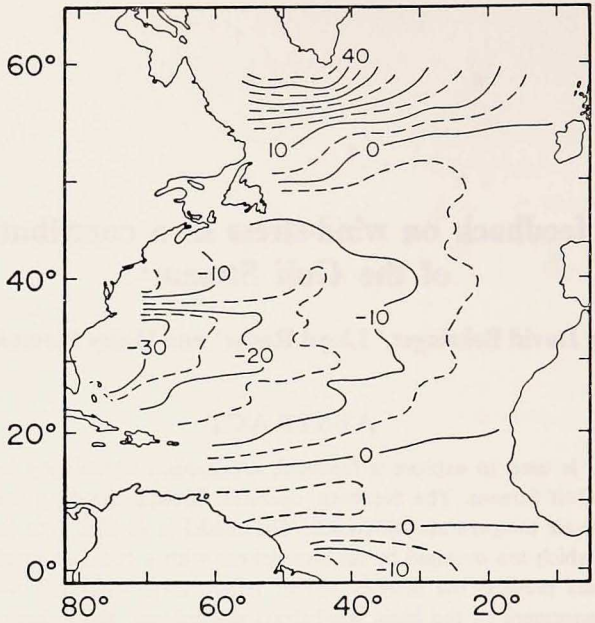

Figure 1. The field of Sverdrup transport computed by Leetmaa and Bunker (1978) showing the Gulf Stream-like current extending from Cape Hatteras to about 50W.

two degrees of latitude and hence the curl of the wind-stress is significantly enhanced near the Gulf Stream.

The drag coefficient is a function of the speed of the wind and the stability of the air (Bunker, 1976). Over the Gulf Stream both higher wind speeds and a greater temperature contrast between the cold air and the warm water contribute to a larger drag coefficient. Leetmaa and Bunker wondered whether the stronger winds somehow reflect the influence of the Stream. This may be so but there is no doubt that the anomalously high sea-air temperature difference is directly associated with the flow of the Gulf Stream and represents part of a feedback loop. A wind-stress pattern leads to a flow field configuration, which leads to a particular distribution of sea surface temperature; the sea surface temperature in conjunction with the air temperature leads, in turn, to a modification of the wind-stress pattern. It should be possible, using a simple model, to examine such a system to discover whether it leads naturally to the formation of an intense Gulf Stream in mid-latitudes.

2. The model

We consider a model which is one dimensional in the sense that the equations have been integrated over the vertical z-direction and over the zonal x-direction so that the variables are functions of the latitude, y, only. The model ocean has an active upper layer of uniform depth, H, which corresponds to an average thermo-

cline depth and interior and western boundary regions of constant widths, W_i and W_b, respectively. The model allows for different meridional temperature distributions in the interior and western boundary by using a pair of coupled equations, one equation for each region.

We begin with an equation for the temperature, T, of an incompressible ocean,

$$\frac{\partial T}{\partial t} = -\left[\frac{\partial(uT)}{\partial x} + \frac{\partial(vT)}{\partial y} + \frac{\partial(wT)}{\partial z}\right] + A_h\left[\frac{\partial^2 T}{\partial x^2} + \frac{\partial^2 T}{\partial y^2}\right] + A_v \frac{\partial^2 T}{\partial z^2}. \tag{1}$$

Heat flows across the surface into the ocean according to a simple Newtonian-type law and hence the surface boundary condition is

$$A_v \frac{\partial T}{\partial z} = -k'(T - T_a)$$

at $z=0$, where T_a is the air temperature. We choose the air temperature to be a linear function of latitude: $T_a(y)=T_0-By$, where T_0 is a representative equatorial air temperature and B is chosen to make T_a decrease toward the northern boundary of the ocean.

For simplicity, we assume that the heat is mixed instantaneously over the depth of the layer and that there is no heat loss through the bottom of the layer. Hence, the bottom boundary condition is

$$A_v \frac{\partial T}{\partial z} = 0$$

at $z=-H$. We also assume that the vertical velocity is zero at $z=0$ and $z=-H$.

Integrating equation (1) over the depth of the layer, we get

$$\frac{\partial \bar{T}}{\partial t} = -k(\bar{T} - T_a) - \left[\frac{\partial(\bar{u}\bar{T})}{\partial x} + \frac{\partial(\bar{v}\bar{T})}{\partial y}\right] + A_h\left[\frac{\partial^2 \bar{T}}{\partial x^2} + \frac{\partial^2 \bar{T}}{\partial y^2}\right] \tag{2}$$

where $k=k'/H$ and the overbars represent vertical averages. The equation for continuity of mass, following the same assumptions, is

$$\frac{\partial \bar{u}}{\partial x} + \frac{\partial \bar{v}}{\partial y} = 0. \tag{3}$$

Before integrating these equations in the x-direction we must specify the appropriate zonal boundary conditions. For the interior region, extending from $x=0$ to $x=W_i$, the boundary conditions are set to allow no flux of mass or heat through the wall: $\bar{u}=0$ and $\frac{\partial \bar{T}}{\partial x} = 0$ at $x=W_i$. By integrating equation (3) from $x=0$ to $x=W_i$, we get the second boundary condition for $\bar{u}$:

$$\bar{u} = W_i \frac{\partial \bar{v}}{\partial y} \qquad \text{at } x=0.$$

Next, we use the condition,

$$A_h \frac{\partial \bar{T}}{\partial x} = \frac{\mu}{W_b}[\bar{T}_i - \bar{T}_b] \qquad \text{at } x=0\,,$$

to represent the mixing of heat between the interior at the temperature, $\bar{T}_i$, and the western boundary at the temperature, $\bar{T}_b$. Finally, we need to specify $\bar{T}$ at $x=0$. In order to do so we distinguish between two regimes as functions of latitude. The distinction is necessary because, in general, the interior and western boundary temperatures are different and the direction of flow between the regions involves one or the other of these two temperatures. In regime I the water flows from the interior into the western boundary current and we set $\bar{T}(x=0)=\bar{T}_i$. In regime II the western boundary current flows into the interior and we set $\bar{T}(x=0)=\bar{T}_b$.

Using these boundary conditions, we can integrate equation (2) from $x=0$ to $x=W_i$ and obtain the model equations for the interior region. We write the equations in terms of the sea-air temperature difference, $\theta=\bar{T}_i-T_a$, and take advantage of the fact that T_a is a linear function of y only.

Regime I $\left(\bar{u}(x=0)<0 \text{ or } \frac{\partial \bar{v}}{\partial y} < 0\right)$.

$$\frac{\partial \theta}{\partial t} = -k\theta - \bar{v}\frac{\partial(\theta + T_a)}{\partial y} + A\frac{\partial^2 \theta}{\partial y^2} - \frac{\mu}{W_i W_b}(\theta + T_a - \bar{T}_b)\,. \tag{4}$$

Regime II $\left(\bar{u}(x=0)>0 \text{ or } \frac{\partial \bar{v}}{\partial y} > 0\right)$.

$$\frac{\partial \theta}{\partial t} = -k\theta - \bar{v}\frac{\partial(\theta + \bar{T}_a)}{\partial y} + A\frac{\partial^2 \theta}{\partial y^2} - \left[\frac{\partial \bar{v}}{\partial y} + \frac{\mu}{W_i W_b}\right](\theta + T_a - \bar{T}_b)\,. \tag{5}$$

In addition to equations (4) and (5) we use the following Sverdrup dynamical relationship:

$$\rho\,\beta\,\bar{v}\,H = -\frac{\partial \tau}{\partial y} \tag{6}$$

where the x-component of the wind-stress is given as

$$\tau = \tau_0(y)\,(1 + \epsilon\theta)\,. \tag{7}$$

In equation (7) the function $\tau_0(y)$ represents the stress in the absence of any effect of sea-air temperature difference, θ, and the expression $(1+\epsilon\theta)$ is introduced as a crude representation of the θ-dependence of the drag coefficient.

In order to close the system it is necessary to specify $\bar{T}_b$. We obtain the equations for $\bar{T}_b$ by integrating equation (2) across the western boundary region from $x=0$ to $x=-W_b$. The boundary conditions are analogous to those in the interior region and we make use of the fact that the northward transport in the western boundary must

balance the southward transport in the interior. There are two equations similar to the equations (4) and (5).

Regime I $\left(\frac{\partial \bar{v}}{\partial y} < 0\right)$.

$$\frac{\partial T_b}{\partial t} = -k(T_b - T_a) + \lambda \bar{v} \frac{\partial T_b}{\partial y} + A_b \frac{\partial^2 T_b}{\partial y^2} + \lambda \left[\frac{\partial \bar{v}}{\partial y} - \frac{\mu}{W_i W_b}\right](T_b - \theta - T_a). \tag{8}$$

Regime II $\left(\frac{\partial \bar{v}}{\partial y} > 0\right)$.

$$\frac{\partial T_b}{\partial t} = -k(T_b - T_a) + \lambda \bar{v} \frac{\partial T_b}{\partial y} + A_b \frac{\partial^2 T_b}{\partial y^2} + \frac{\lambda \mu}{W_i W_b}(\theta + T_a - T_b). \tag{9}$$

In equations (8) and (9) $\lambda = W_i / W_b$.

Equations (6), (7) and either of the combinations of (4) and (8) or (5) and (9), depending on the sign of $\frac{\partial \bar{v}}{\partial y}$, describe the system. Because $\bar{v}$ is a function of θ (through the thermally sensitive drag coefficient), the products of $\bar{v}$ and θ and their derivatives in equations (4) and (5) introduce an essential nonlinearity into the problem. The fact that there are two regimes, I and II, whose distribution in y at any time is determined by the instantaneous field of $\frac{\partial \bar{v}}{\partial y}$ also is strongly nonlinear.

In our calculations the basic value of $\tau_0(y)$ is taken as

$$\tau_0(y) = -\frac{\tau_0}{\rho} \cos\left[\frac{m\pi}{L} y\right]$$

where L is the meridional dimension of the basin. The form of the wind-stress can yield a two-gyre ocean ($m=2$) with both subpolar and subtropical gyres. The boundary conditions at the northern and southern ends of the ocean are $\bar{v}=0$ and $A \frac{\partial T_i}{\partial y} = 0 \left(\text{or } \frac{\partial \theta}{\partial y} = B\right)$.

Solutions have been obtained numerically by a simple time-step integration of equations (4), (5), (8) and (9), continuing until the time-rate of change of the θ-field becomes zero. We perform the time integration starting with $\theta=0$. A table for $\bar{v}$ is computed from equation (6) using the instantaneous value of $\tau(y)$ which at the first time step is simply $\tau_0(y)$. Once θ has been stepped forward, the new values of $\tau(y)$ are computed from equation (7) and the $\bar{v}$-table is recomputed from equation (6).

In the experimental results which follow, the final distributions of θ generally show that the gyre interiors gain heat from the air in the south and lose heat to the air farther north. In our discussion we treat this pattern of heat gain and loss in the

Table 1. Diffusivity coefficients for the experiments α_1 through α_6. The units are $cm^2\ sec^{-1}$.

Exp.	α_1	α_2	α_3	α_4	α_5	α_6
A	0	1×10^7	4×10^7	1×10^7	1×10^7	1×10^7
A_b	$.85\times10^7$	1×10^7	4×10^7	1×10^7	1×10^7	1×10^7
μ	4×10^6	4×10^8	4×10^6	0	4×10^8	16×10^8

interior as essentially that of the basin as a whole. We can reasonably do this because, although the sea-air temperature difference in the western boundary can be greater than in the interior, the relative narrowness of the western boundary means that at any latitude the total heat exchange in the western boundary is only a few percent of the interior value.

3. The experiments

Since there are two sources of nonlinearity there are some interesting effects to be found even for the case of no feedback: $\epsilon=0$. Accordingly, we will first discuss this case. It yields some idea of the magnitude of the diffusivity required to transport properties from the southern to the northern gyre, which would otherwise be isolated.

The case $\epsilon=0$. In order to illustrate the nature of the sea-air temperature difference, θ, in a two gyre ocean a series of experiments were run using the diffusivity coefficients in Table 1. Otherwise, all of the experiments have the common parameters:

$\epsilon=0$, $k=8\times10^{-9}\ sec^{-1}$, $H=1$ km, $L=6000$ km, $W_i=3000$ km,
$W_b=100$ km, $\tau_0=1$ dyne cm^{-2}, $T_0=17°C$, $B=2.83\times10^{-3}\ °C\ km^{-1}$,
and the y-grid dimension is 36 points.

The results are shown in Figure 2. Since the applied stress, τ, is a simple cosine function, the Sverdrup transport (velocity $\bar{v}$) is also trigonometric and, in the case $\epsilon=0$, it is wholly unaffected by the sea-air temperature difference.

In experiment α_1 there was no meridional diffusion in the interior and hence no heat transport between the two gyres except indirectly due to the small meridional diffusion in the western boundary current. A large temperature discontinuity (in θ) exists between grid points 18 and 19, at the boundary between the two noncommunicating gyres.

Curve α_1 shows large north-south asymmetry in each gyre. The amplitude of θ is greatest in the regimes II where the water from the western boundary currents enters the interior. Overall heat balance is nearly maintained separately in each gyre. Virtually all the heat that is absorbed from the air in each gyre is released again within the same gyre at a more northern latitude. The extent in latitude of the region of heat absorption in the subtropical gyre is greater than that in which it is given up again. The maximum meridional transport of heat by the combined gyre

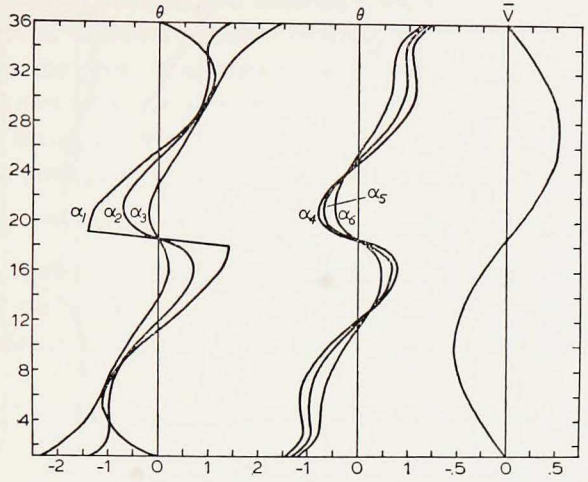

Figure 2. The sea-air temperature difference, θ, and the interior Sverdrup velocity, $\bar{v}$, for the experiments α_1 through α_6. The units are degrees Celsius and cm sec^{-1}, respectively. All experiments have $\epsilon=0$. The remaining parameters are given in the text.

and western boundary current system does not coincide with the maximum meridional mass transport of each gyre, but in both gyres occurs somewhat nearer to midlatitude. In the interior there is no heat transport across the latitude bounding the two gyres.

The curves for experiments α_2 and α_3 show the sea-air temperature difference for two choices of the meridional diffusivity ($A=A_b = 1\times10^7$, 4×10^7 cm^2 sec^{-1}). The temperature discontinuity is removed. For the larger value of A in experiment α_3 heat absorbed from the air at low latitudes is almost entirely transferred to high latitudes across the boundary between the gyres by the eddy diffusion.

Looking at the qualitative features of Bunker's (1976) heat balance charts one gets the impression that most of the heat absorbed in the subtropical gyre of the North Atlantic is released in the northern portion of the subtropical gyre and that only something less than half of it is transferred to the subpolar gyre. In this model it would require a diffusivity coefficient as in experiment α_1 to accomplish this.

The need for transfer between gyres is even more clear when one considers the oceanic fresh water balance. Because there is net evaporation over the subtropical gyre and net precipitation over the subpolar gyre, there would be no realistic steady state solution to our model in the absence of transport between the gyres. Eventually, the water would become so saline that its density would exceed that of the subpolar gyre.

The remaining curves in Figure 2 show the effect on the sea-air temperature difference of variations in the eddy diffusivity between the western boundary and the interior. The curve α_4 shows θ for an experiment in which there is no zonal

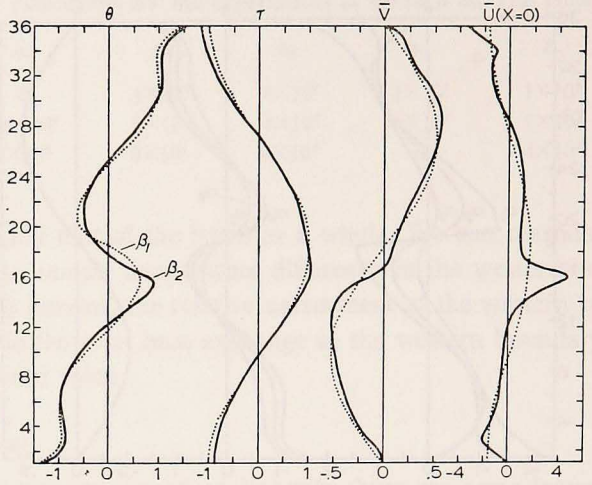

Figure 3. The sea-air temperature difference, θ, the wind-stress, τ, the Sverdrup velocity, $\bar{v}$, and the zonal velocity, $\bar{u}(x=0)$, for the experiments β_1 and β_2. The units are degrees Celsius, dynes cm^{-2}, cm sec^{-1}, and cm sec^{-1}, respectively. Experiment β_1 has $\epsilon=0$ and experiment β_2 has $\epsilon=0.125$. The remaining parameters are given in the text.

eddy diffusion; heat is transferred between the regions by advection alone. The curves α_5 and α_6 show that when diffusion is included ($\mu=4\times10^6$, 16×10^6 cm^{2}sec^{-1}) the amplitude of θ is reduced. In the subtropical gyre the diffusion has caused a warming of the southern interior and a cooling of the western boundary current which, in turn, has led to a less effective warming of the northern interior by the outflow of the western boundary current. This effect has its mirror image in the subpolar gyre.

The net effect of the diffusion between the western boundary and the interior is to partially short-circuit the oceanic flux of heat. Nevertheless, for reasonable values of μ this effect is less important in determining the nature of the solutions than the transfer of heat between the gyres.

The case $\epsilon\neq0$. With $\epsilon\neq0$ we have the possibility of feedback of the sea-air temperature difference upon the wind-stress, and the tendency for the development of a jet, or "Gulf Stream" at mid-latitudes. Figure 3 shows the results of two experiments with the two gyre system. The parameters are the same as in the previous case, except the diffusivity coefficients are $A=1\times10^7$ cm^2 sec^{-1}, $A_b=4\times10^7$ cm^2 sec^{-1} and $\mu=4\times10^6$ cm^2 sec^{-1}. The curve β_1 has zero ϵ and represents a control experiment. In curve β_2 some feedback is introduced ($\epsilon=0.125$) so that the stress is enhanced somewhat where θ is large. The maximum stress—which in the absence of feedback is between points 18 and 19—is displaced southward to between points 16 and 17

due to the high sea-air temperature difference there. This distorts the Sverdrup velocity, $\bar{v}$, as shown, so that it vanishes between points 16 and 17. There is also a northward shift of the point of maximum meridional velocity in each gyre: in the subtropical gyre from point 10 to point 12 and in the subpolar gyre from point 27 to point 28. The maximum velocity in the subpolar gyre is also increased by about 8%. In the subtropical gyre the displacement of the maximum $\bar{v}$ and of the vanishing $\bar{v}$ has a large effect upon $\frac{\partial \bar{v}}{\partial y}$ and, consequently, upon the eastward flowing current from the western boundary into the interior. As can be seen in Figure 3 the zonal current in the subtropical gyre has been halved in width and more than doubled in amplitude forming a jet in the region of the Leetmaa-Bunker Gulf Stream.

Zonal jets also form in the extreme north and south where the insulating boundary conditions $\left(\frac{\partial T_i}{\partial y} = 0\right)$ permit the buildup of large sea-air temperature differences. If the boundary conditions were changed to $\frac{\partial \theta}{\partial y} = 0$, then there would be a flux of heat across the boundaries from south to north which in the absence of advection would maintain the initial oceanic temperature distribution ($T_i = T_a$). At the southern boundary this could be considered to be a rough simulation of the cross-equatorial heat flux during the northern hemisphere winter. We reran the experiments shown in Figure 3 using these flux boundary conditions and, as expected, the sea-air temperature difference at meridional boundaries was reduced by nearly 70% and the zonal jets there were eliminated. However, in the vicinity of the "Gulf Stream", changes in all fields were no more than a few percent. The choice between the boundary conditions, $\frac{\partial T_i}{\partial y} = 0$ and $\frac{\partial \theta}{\partial y} = 0$, evidently has little effect on the formation of the model "Gulf Stream" at mid-latitudes.

If we attempt to compute results for larger ϵ, reversals in the sign of $\frac{\partial \bar{v}}{\partial y}$ begin to appear in the vicinity of the zonal jets and these introduce additional gyres which are resolved by only one or two grid points. Therefore, we doubled the number of grid points to 72 before running additional experiments for larger ϵ. The basic parameters for these experiments were the same as for the previous experiments, except that now $A_b = 8 \times 10^7$ cm^2 sec^{-1}. Experiments using the insulating condition $\left(\frac{\partial T_i}{\partial y} = 0\right)$ at the meridional boundaries developed a small third gyre south of the subtropical gyre and very strong zonal jets at the meridional boundaries. For example, an experiment with $\epsilon = 0.25$ formed a third gyre which had an eastward jet with a maximum speed of 8.7 cm sec^{-1} and a westward jet at the northern boundary with a maximum speed of 10.6 cm sec^{-1}. Both of these exceeded the

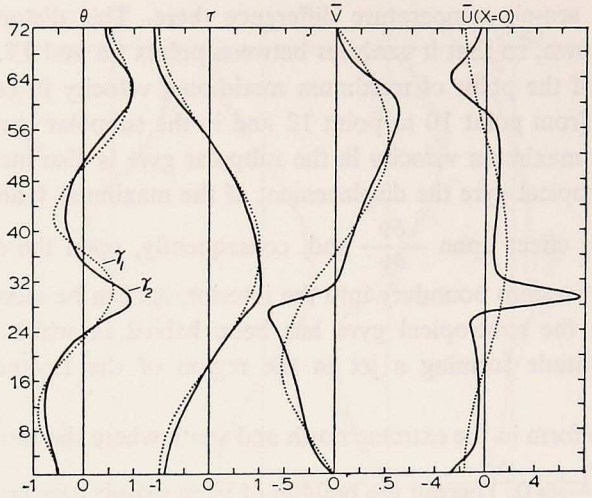

Figure 4. The same as in Figure 3, except for experiments γ_1 and γ_2. Experiment γ_1 has ϵ=0 and experiment γ_2 has ϵ=0.25.

maximum speed of 6.9 cm sec^{-1} in the model "Gulf Stream". Comparable experiments using the flux boundary $\left(\frac{\partial \theta}{\partial y} = 0\right)$ again had essentially the same "Gulf Streams" but developed neither the third gyre nor the boundary jets. Figure 4 shows the results of two of these experiments. The curve γ_1 has ϵ=0 and represents the control experiment. In experiment γ_2 enough feedback has been introduced (ϵ=0.25) so that the wind-stress in the vicinity of point 29 has been enhanced by about 23%, comparable to the wintertime enhancement of the stress computed by Leetmaa and Bunker (1978) over the Gulf Stream. The results are much the same as in Figure 3—allowing for the difference in boundary conditions—except for the striking increase of about 30% in the maximum Sverdrup velocity in the subtropical gyre.

Further increases in ϵ eventually cause the calculations to become numerically unstable. We have not found an instance of a stable solution with more than three gyres. Neither have we found an instance of a stable but unsteady solution.

4. Conclusion and comments

Thermal feedback, through the drag coefficient, appears to be capable of producing a "Gulf Stream" without higher order dynamics. There may be other phenomena that can be produced by such a feedback: propagating waves, multiplication of gyres and generation of recirculations, and nonsteady (climate-related?) solutions. These can be explored by further, more sophisticated numerical experimentation.

Two dimensional ocean models deserve attention, and more thought is needed

concerning distinctions between different kinds of layer depths: Ekman layers, mixed layers, and above-the-thermocline layers. The idea that sea-air temperature differences, through feedback upon the drag coefficient, can modify circulation patterns is not new; it has been used previously by Emery and Csanady (1973) to explain the direction of the circulation of lakes under uniform winds through heat transport by Ekman drift.

Acknowledgments. The authors would like to acknowledge their debt to Andrew Bunker's stress calculations as the source of some of these speculations, to Mrs. Mary Hunt for compiling the first version of the computer program, and to the National Science Foundation for the support that made the work possible. We are grateful for stimulating conversations with Drs. Pearn Niiler and Joseph Pedlosky.

REFERENCES

Bunker, Andrew F. 1976. Computations of surface energy flux and annual air-sea interaction cycles of the North Atlantic Ocean. Mon. Weather Rev., *104,* 1122–1140.

Emery, K. O. and G. Csanady. 1973. Surface circulation of lakes and nearly land-locked seas. Proc. Nat. Acad. Sci., *70,* 93–97.

Leetmaa, Ants and Andrew F. Bunker. 1978. Updated charts of mean annual wind-stress, convergences of the Ekman layers, and Sverdrup transports in the North Atlantic. J. Mar. Res., *36,* 311–322.

Stommel, Henry, Pearn Niiler, and David Anati. 1978. Dynamic topography and recirculation of the North Atlantic. J. Mar. Res., *36,* 449–468.

Received: *13 June, 1978;* revised: *15 August, 1979.*